Appl. Phys. B 63, 491–498 (1996)

Applied Physics B Lasers and Optics

© Springer-Verlag 1996

Phase measurements in nonlinear optics

R. Stolle[1,*], G. Marowsky[1], E. Schwarzberg[2], G. Berkovic[2]

[1] Laser-Laboratorium Göttingen e.V., Hans-Adolf-Krebs-Weg 1, D-37077 Göttingen, Germany
(Fax: + 49-551/503599, E-mail: gmanows@gwdg.de)
[2] Department of Materials and Interfaces, Weizmann Institute of Science, Rehovot, 76100, Israel

Received: 23 January 1996/accepted: 11 June 1996

Abstract. Measurement of the phase, and not only the intensity, of the nonlinear optical response of a system is important in many applications which are reviewed here. We demonstrate and compare several techniques for direct measurement of the phase of the nonlinear susceptibilities through nonlinear interferometry. Different ways of imparting a controllable phase shift are discussed. Unless the coherence length is impractically large, the preferred method is to use a variable-pressure gas cell to control the phase difference between the input laser pulse and the nonlinear optical signal.

PACS: 0760; 4260H; 4265

Since the mid-1980s, second-order nonlinear optical methods – notably Second-Harmonic Generation (SHG) and Sum Frequency Generation (SFG) – have received considerable attention as a means of probing numerous media, and in particular surfaces and thin films [1–3]. In these methods, one detects radiation generated at a frequency equal to the sum of the frequencies of two laser photons incident on the material. SHG and SFG depend on the second-order susceptibility $\chi^{(2)}$ (also known as nonlinear polarizability) of the medium. Under the electric dipole approximation [1], $\chi^{(2)}$ as a third-rank tensor is zero in a centrosymmetric medium. At a surface or interface between centrosymmetric media, the inversion symmetry is necessarily broken, and thus $\chi^{(2)}$ processes are inherently specific to the surface.

When irradiated by laser light at frequencies ω_1 and ω_2, a nonlinear polarization at the sum frequency is created according to

$$\text{(SFG)}\quad P^{(2)}(\omega_1+\omega_2)=\chi^{(2)}(\omega_1+\omega_2;\omega_1,\omega_2)E(\omega_1)E(\omega_2), \tag{1}$$

which for the degenerate case $\omega_1=\omega_2$ leads to second-harmonic generation

$$\text{(SHG)}\quad P^{(2)}(2\omega)=\chi^{(2)}(2\omega;\omega,\omega)E(\omega)E(\omega). \tag{2}$$

SHG and SFG have several advantages and attractive features relative to other surface probing techniques:

- They are applicable to all interfaces accessible by light.
- The signal is coherent and monochromatic, enabling easy spatial and spectral filtering from background and scattered radiation.
- They have the same high temporal and spatial resolution as that offered by lasers.
- The use of tunable lasers enables surface spectroscopy.
- The experimental setup is relatively simple, in particular in the case of SHG.

Consequently, these techniques have been applied to probe numerous surfaces of crystals, glasses, metals, semiconductors and liquids, and the interfaces between them. Several comprehensive reviews have been given in [1, 2].

In most cases, the *magnitude* of a SHG (SFG) signal is measured which can provide much useful information regarding adsorbates at surfaces – including coverage density and orientation – and surface symmetry. However, by only measuring the magnitude of this signal, information regarding its phase is necessarily lost. The phase of the nonlinear polarizability can be thought of as the phase of the SHG or SFG wave relative to the input wave(s) at the time of creation. Since $\chi^{(2)}$ in (1) and (2) can be complex valued, a phase difference can arise. Geometrical factors, like the nonlinear Fresnel factors [4], can also give rise to a phase difference.

We shall review here methods of how the phase of the nonlinear susceptibility $\chi^{(2)}$ can be determined. We illustrate with several examples – primarily with SHG – how the knowledge of the phase leads to additional important

* *Present address*: Research Institute for Materials, University of Nijmegen, Toernooiveld, NL-6525 ED Nijmegen, The Netherlands. E-mail: rstolle@sci.kun.nl

Dedicated to Prof. F. P. Schäfer on the occasion of his 65th birthday.

information which is not conveyed when only the magnitude of $\chi^{(2)}$ is measured.

1 Theory and coherence length

In general, phase information about $\chi^{(2)}$ can be obtained by either "direct" or "indirect" methods. We can identify as an "indirect" method techniques [5–7] where phase differences between individual components of the $\chi^{(2)}$-tensor of the same species are inferred, or fitted from a series of measurements, each probing different weights and combinations of elements of the $\chi^{(2)}$-tensor.

In a "direct" measurement, the phase of $\chi^{(2)}$ is observed directly through an interferometric technique as originally introduced by Chang et al. [8]. In these experiments, the second-harmonic signal generated by the sample, $E_{\text{sam}}^{(2\omega)}$, is superimposed by another signal of a second (reference) SH source, $E_{\text{ref}}^{(2\omega)}$. A variation of the optical phase delay between these two sources is introduced by using a Phase-Shifting Unit (PSU) and results in an interference pattern from which the phase of the susceptibility can be deduced. The principle of these experiments is shown in Fig. 1. The total phase difference, Φ, between the two harmonic waves consists of the (constant) contributions Φ_{sam} and Φ_{ref}, introduced by the sample and reference, and a variable phase shift, Φ_{PSU}, due to the PSU:

$$\Phi = \Phi_{\text{sam}} + \Phi_{\text{PSU}} + \Phi_{\text{ref}}. \tag{3}$$

Provided there is perfect spatial and temporal coherence, the total SH signal, I_{tot}, is given by

$$I_{\text{tot}} \propto |E_{\text{sam}}^{(2\omega)} + E_{\text{ref}}^{(2\omega)}|^2$$

$$= I_{\text{sam}} + I_{\text{ref}} + 2\sqrt{I_{\text{sam}} I_{\text{ref}}}\cos\Phi, \tag{4}$$

with $I_{\text{sam}} \propto |E_{\text{sam}}^{(2\omega)}|^2$ and $I_{\text{ref}} \propto |E_{\text{ref}}^{(2\omega)}|^2$ being the SH signals from the sample and the reference. It is possible to deduce the value of Φ_{sam}, i.e. the phase of the unknown susceptibility, if either (i) Φ_{ref} is known and Φ_{PSU} can be extrapolated to zero, or (ii) if both Φ_{ref} and Φ_{PSU} are unknown and the experiment is compared with a standard sample of known susceptibility, e.g. quartz [9]. In such a nonlinear-optical interference experiment, not only the phases of the unknown susceptibilities can be determined but it is also possible to study the dispersion characteristics of the PSU and the temporal and spatial coherence of the laser.

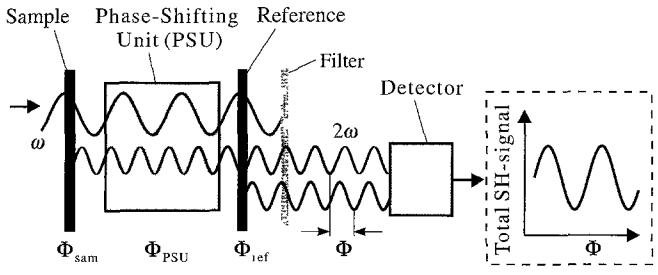

Fig. 1. Setup schematic for second-harmonic phase measurements. The beam displacement has been added for clarity

A PSU can be realized in many ways, depending on the expected *coherence length*, l_c. In nonlinear optics, the coherence length is a measure of the distance over which the fundamental wave and the nonlinear signal wave get out of phase by π. The value of l_c depends on the particular nonlinear-optical process, the frequency of the incident wave(s) and also on the dispersion characteristics of the PSU. In the case of second-harmonic generation, l_c^{SHG} is given by [10]

$$l_c^{\text{SHG}} = 2\pi/\Delta K, \tag{5}$$

with the phase mismatch $\Delta k = k(2\omega) - k(\omega)$ of the wave numbers $k(\omega)$ and $k(2\omega)$ of the fundamental and the harmonic radiation.

2 Methods

In the following we shall introduce four possibilities of realizing a PSU, namely (a) gas cell, (b) variation of the distance between both SH sources, (c) rotating plate and (d) a pair of glass wedges.

(*a*) *Gas cell.* A common realization of a PSU is a gas cell with variable gas pressure p, as originally introduced by Chang et al. [8]. Either the gas cell is placed between both SH sources (Fig. 2a) or it contains both sources (Fig. 2b). A variation of p results in the dispersion, $\Delta n(p) = n(2\omega, p) - n(\omega, p)$, according to $\Delta n(p) = \Delta n_0(p/p_0)$, with Δn_0 being the dispersion at standard pressure, p_0. Figure 2c shows a typical interferogram for a 36 cm gas cell filled with air, placed between two quartz plates as SH sources. The data can be nicely fitted by the function

$$I_{\text{tot}} = C_1 + C_2\cos\left(\frac{2\pi}{\Delta p}\,p + \Phi\right), \tag{6}$$

with the periodicity parameter

$$\Delta p = \frac{\lambda p_0 T}{2\Delta n_0 L T_0} \tag{7}$$

at the gas temperature T, the standard temperature $T_0 = 273.15$ K, the cell length L and the fundamental wavelength λ. The parameter Φ is relevant for determining the phase of the susceptibility Φ_{sam} of the sample: either Φ_{ref} is known, and both sample and reference are placed within a gas cell so the variable phase shift Φ_{PSU} can be extrapolated to zero (see Fig. 2b), or the experiment has to be compared using a standard SH source of known susceptibility. The parameters C_1 and C_2 depend on both the signal strength of each single SH source and the laser coherence as shown in Sect. 3.3. The periodicity parameter Δp can be used to determine the dispersion Δn_0 of the gas with extremely high accuracy [11]. In Fig. 2c, the value $\Delta p \approx 290$ Torr corresponds to the dispersion of air $\Delta n_0 = n(1064\text{ nm}) - n(532\text{ nm}) = 39 \times 10^{-7}$, equivalent to a coherence length $l_c = \lambda/(2\Delta n_0) \approx 13$ cm. In summary, the use of a gas cell as PSU is advantageous provided the length of the gas cell is comparable to the coherence

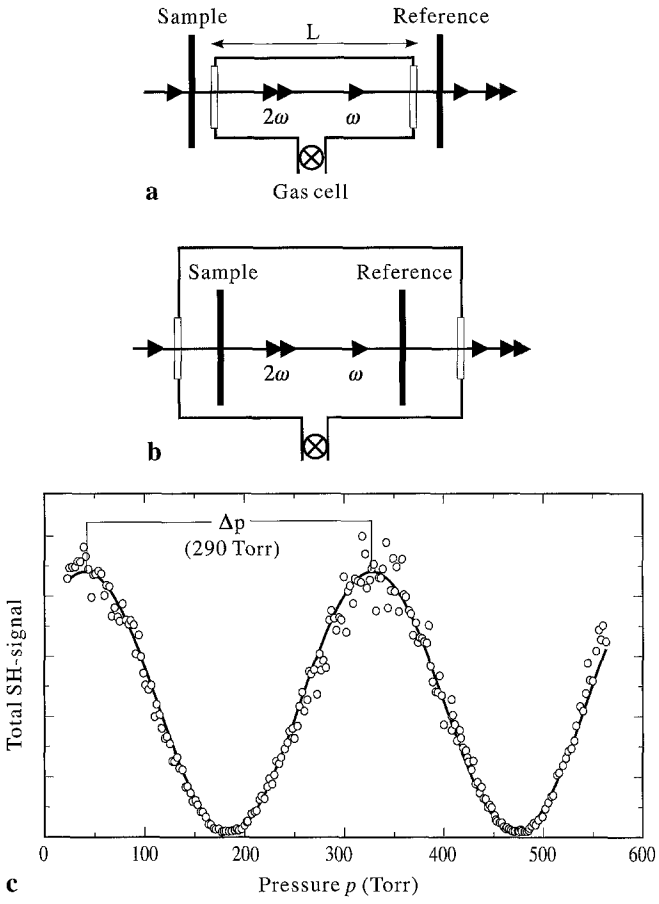

Fig. 2. Two possible configurations for use of a gas cell as PSU. The cell is either placed between sample and reference (**a**) or it contains both SH sources (**b**). Figure 2c shows an interferogram if a 36 cm long gas cell is used (configuration **a**). Data were taken with a Q-switched Nd : YAG laser at 1064 nm, using two quartz plates as SH sources

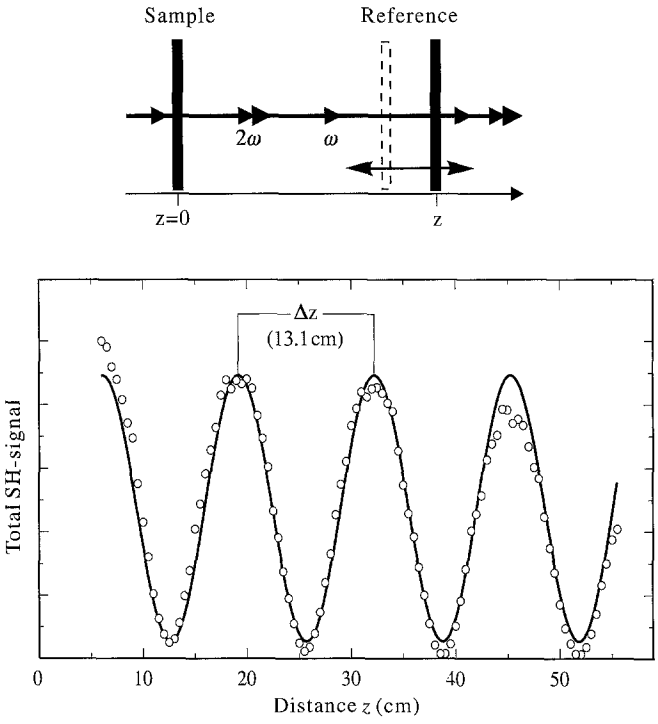

Fig. 3. Variation of the distance between sample and reference in air. Data were taken with a Q-switched Nd : YAG laser at 1064 nm, using two quartz plates as SH sources

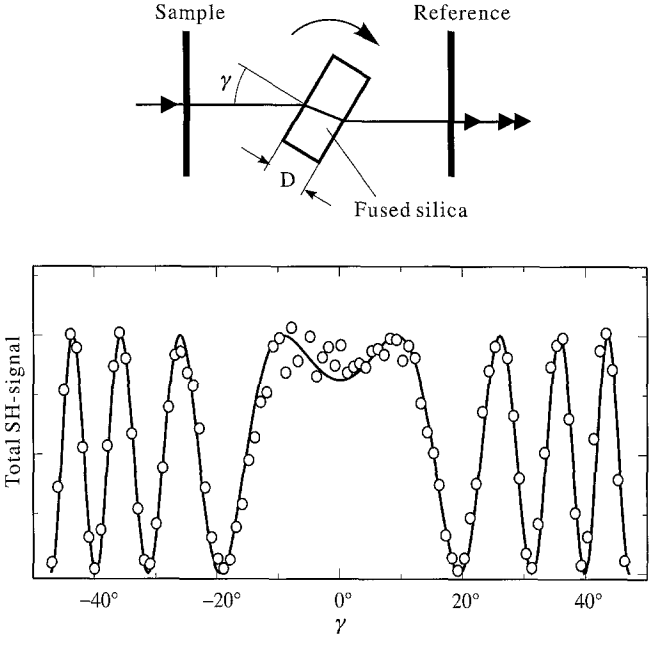

Fig. 4. Rotatable dispersive 1 mm thick plate made of BK7 glass used as PSU. Data were taken with a Q-switched Nd : YAG laser at 1064 nm, using two quartz plates as SH sources

length. It offers the advantage of no moving parts, no beam displacement or generation of additional divergence, and the data can be easily analysed using a simple cosine function.

(*b*) *Variation of the distance.* The dispersion of air can also be used by varying the distance between the two SH sources (see Fig. 3). The periodicity parameter Δp is equal to the coherence length l_c. Therefore, the translation of one of the SH sources may be impracticable when using a Nd : YAG laser at 1064 nm, since a translation of about 13 cm is required to obtain just one interference cycle. Apart from space constraints, the divergence of the laser leads to other problems because the contribution of the translated source will vary during the experiment, and thus the data cannot be fitted by simply using (6) as shown in Fig. 3. On the other hand, it is simple to extrapolate Φ_{PSU} to zero just by extrapolating to zero the distance between the sample and the reference.

(*c*) *Rotating plate.* Another realization of a PSU is the use of a rotatable (dispersive) plate made of glass or fused silica between the sample and the reference [12] as shown in Fig. 4. This experimental setup overcomes the space constraints mentioned above [13], but introduces a slight beam displacement and may cause weak additional SH radiation generated at the tilted surface of the plate. The complex interference pattern is approximately given

by [14]

$$I_{\mathrm{rot}}(2\omega) = C_1 + C_2 \cos[4\pi(D/\lambda)(n_{2\omega}\cos\gamma_i^{2\omega} - n_{\omega}\cos\gamma_i^{\omega}) + \Phi], \quad (8)$$

with the plate thickness D, the wavelength λ of the fundamental radiation and with $\gamma_i^{2\omega}$ and γ_i^{ω} being the angles of refraction of the harmonic and the fundamental beam inside the plate, which can be calculated using $\gamma_i^{\Omega} = \arcsin[\sin(\gamma)/n(\Omega)]$ (Fig. 4). The dispersion of glass or fused silica is many orders of magnitudes larger than that of any gas. Thus, for nonlinear optical processes like Difference-Frequency Generation (DFG) or Coherent Anti-Stokes Raman Scattering (CARS) with very large coherence lengths in air, this technique may be useful.

Using a periodically rotating plate in combination with a lock-in amplifier, Thiansathaporn and Superfine [15] demonstrated the application of Homodyne SHG (HSHG). This technique provides real-time measurements of the phase and the magnitude of susceptibilities, and an improvement in the signal-to-noise ratio [15].

(*d*) *Pair of wedges.* The disadvantages concerning beam displacement and a complicated interference pattern may be overcome by using a pair of wedges of adjustable thickness as shown in Fig. 5. The obtained data can easily be described by a cosine function as in the case of the gas cell. This technique is suitable for experiments with a very long coherence length which may occur for example in DFG or CARS. Figure 5 shows the result of a CARS experiment with atmospheric oxygen [16]. In this case, the coherence length would be about 3 m in air as compared to only $l_c \approx 910$ μm in BK7 glass.

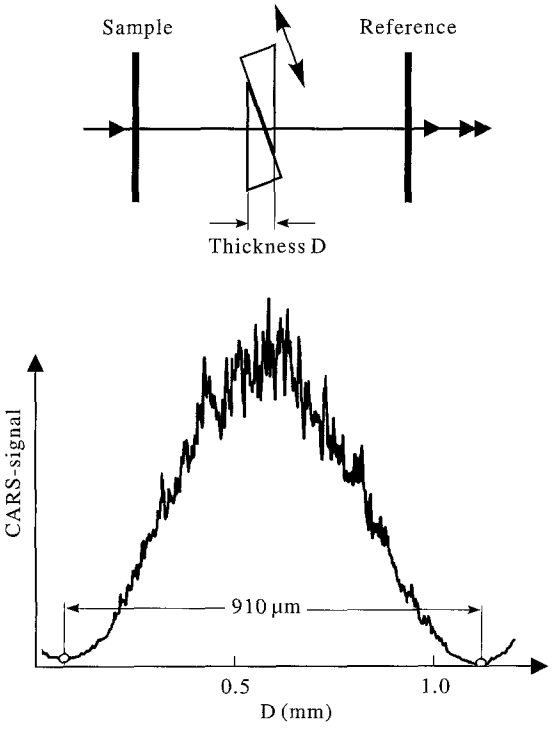

Fig. 5. PSU made from a pair of wedges of BK7 prisms of adjustable thickness. Data were taken from a CARS experiment with atmospheric oxygen [16]

Comparison of the methods. We have seen that a PSU in a nonlinear-optical interference experiment can be realized in various ways. In order to choose the best suitable method, one has to estimate the expected coherence length, which depends strongly on the particular experiment. In second-harmonic experiments with the fundamental in the VIS/IR region, the dispersion of air is sufficient for the use of a gas cell. Using a gas cell offers the advantage of no moving parts, no beam displacements or generation of additional divergence and an interference pattern which can be readily interpreted. In a difference-frequency-type experiment like DFG or CARS, the use of higher dispersive media like glass or fused silica may be necessary.

3 Selected examples

We shall illustrate uses of SHG phase measurements and interferometry with several examples from our research groups and other laboratories. These examples include the use of phase-sensitive SHG as a probe for molecular directionality at surfaces and also the correct interpretation of a SH experiment when susceptibilities of different species contribute to the total SH signal. We also use phase-sensitive SHG for the measurement of coherence properties of lasers. New approaches for phase measurements in dispersive geometries are discussed. Finally, we briefly survey numerous other experiments where phase control between fundamental laser radiation and harmonic response is employed.

3.1 Background suppression and addition of susceptibilities

When two (or more) species contribute to a surface signal, the total SHG intensity measured can depend on the relative phase between them. Consider a surface where both the substrate (sub) and adsorbate (ads) species contribute to the total SHG. The measured SHG intensity will be proportional to $|\chi^{(2)}_{\mathrm{tot}}|^2$ with $\chi^{(2)}_{\mathrm{tot}} = \chi^{(2)}_{\mathrm{sub}} + \chi^{(2)}_{\mathrm{ads}} + \chi^{(2)}_{\mathrm{int}}$. The latter term, $\chi^{(2)}_{\mathrm{int}}$, which corresponds to the interaction of substrate and adsorbate, will be ignored in the following, although it has been shown that for many experiments it has to be taken into account for a correct interpretation of the data [17–20].

Depending on the phase difference between $\chi^{(2)}_{\mathrm{sub}}$ and $\chi^{(2)}_{\mathrm{ads}}$, the total SHG signal will show different behaviour as the ratio $|\chi^{(2)}_{\mathrm{sub}}|/|\chi^{(2)}_{\mathrm{ads}}|$ is varied. In Fig. 6, we show typical behaviour for phase differences of 0, $\pi/2$ and π between $\chi^{(2)}_{\mathrm{sub}}$ and $\chi^{(2)}_{\mathrm{ads}}$. Note that within a given system, the ratio $|\chi^{(2)}_{\mathrm{sub}}|/|\chi^{(2)}_{\mathrm{ads}}|$ can be varied, e.g. by changing the adsorbate concentration or degree of alignment. For off-resonance SHG studies, $\chi^{(2)}$ must be real so phases can only be either 0 or π – nevertheless the effect of phase can be striking by comparing the plots for these two cases. Zero phase difference leads to a "normal" quadratic increase of SHG with $\chi^{(2)}_{\mathrm{ads}}$, while for a phase difference of π, SHG cancellation

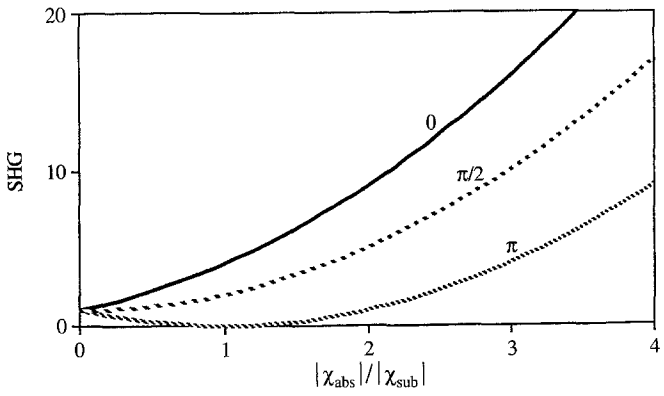

Fig. 6. Total SH signal as a function of the ratio $\chi^{(2)}_{ads}/\chi^{(2)}_{sub}$ for various phase differences (0, $\pi/2$ and π) between $\chi^{(2)}_{ads}$ and $\chi^{(2)}_{sub}$. The vertical scale of SH intensity is normalized to a value of 1 for the bare substrate

can occur. We have indeed observed such behaviour in the concentration-dependent SHG signal for a cyano-biphenyl molecule (8CB) on glass, and directly verified the π phase shift in the nonlinear susceptibilities of glass and 8CB by measuring the phase of total $\chi^{(2)}$ at concentrations above and below the cancellation point [21]. In another study [22], we have observed behaviour corresponding closely to the curve for a $\pi/2$ phase shift for a liquid crystal cell. Here, the substrate (Indium Tin Oxide (ITO) coated glass) had an imaginary $\chi^{(2)}_{sub}$ because of ITO absorption at the harmonic wavelength. Furthermore, phase-controlled superposition of an appropriately selected reference signal enabled us to suppress the non-resonant background in anti-Stokes Raman scattering [16].

3.2 Molecular directionality

The measurement of the phase of the nonlinear susceptibility of surface molecules allows the determination of their absolute directionality [9]. Consider the case of an oriented layer of nonlinear active molecules on a substrate. Neglecting local field effects, the macroscopic surface nonlinear susceptibility $\chi^{(2)}$ can be written as the sum of the nonlinear polarizabilities $\beta^{(2)}$ of the molecules, averaged over the molecular orientation

$$\chi^{(2)} = N\langle\beta^{(2)}\rangle, \tag{9}$$

where N is the number of molecules per unit area. Since the microscopic polarizability $\beta^{(2)}$ – as well as the macroscopic susceptibility $\chi^{(2)}$ – is a third-rank tensor, an inversion operation in the molecules will induce a sign reversal of $\chi^{(2)}$, i.e. a π change of the phase of the nonlinear susceptibility. Therefore, a comparison of the phases of $\beta^{(2)}$ and $\chi^{(2)}$ provides information on the absolute molecular directionality with respect to the surface normal. By performing such experiments, Kemnitz et al. [9] determined the absolute directionality of phenol on the surface of an aqueous solution and determined that the OH group points out of the water. Studies disclosing the orientation of submerged hemicyanine layer in a Langmuir-Blodgett multilayer structure have been reported by Sato et al. [23, 24]. A rotating fused silica plate was used as PSU, covered on both sides with layers of the hemicyanine investigated.

Recently, phase-sensitive experiments have also been performed on Nematic Liquid Crystal (NLC) cells [14, 22]. These cells consist of two glass slides coated with a layer of transparent and conductive ITO separated by mylar spacers of a few μm thickness. The ITO sides of the two glass slides are coated with rubbed polyimide layers which provide a homogeneous alignment of the NLC molecules parallel to the rubbing direction in the absence of any applied field. An external DC electric field, E, normal to the glass slides induces a dipole moment, and the NLC molecules tend to orient themselves parallel to this field. However, the underlying second-order nonlinear susceptibility of the molecules, $\chi^{(2)}$, is proportional to the applied electric field: $\chi^{(2)} \propto E$ [25]. Consequently, the sign of $\chi^{(2)}$ is directly related to the sign of E. Based on this assumption, a phase shift of π in the harmonic field generated by the bulk NLC molecules should be expected upon sign reversal of the electric field. We checked this by performing a phase measurement with an NLC cell (ZLI-1565 by Merck) of 5 μm thickness and an applied voltage of $\pm$ 25 V. Figure 7 shows the experimental setup and two interferograms for $\pm$ 25 V. They have a phase difference of π whereas the signal strengths are nearly identical, as predicted by theory. Time-resolved experiments are in progress to identify the physical nature and kinetics of the observed sign reversal of the susceptibility $\chi^{(2)}$ – molecular reorientation or fast electronic changes in the sign of the induced dipole moment.

3.3 Laser coherence

In other studies we have used the interferogram of an SHG phase measurement to characterize the laser coherence [3]. We first recognize that the interference of two SHG signals is given by (4) only in the case of a plane wave, which is not realistic for lasers in any case. However, it was shown [26] that this equation is valid for a single-mode Gaussian laser beam. For multimode lasers, the laser field is not perfectly coherent, and the interferogram should be described by the modified equation

$$I = I_{sam} + I_{ref} + 2\alpha_1\alpha_2\sqrt{I_{sam}I_{ref}}\cos\Phi. \tag{10}$$

However, α_1 describes the temporal coherence of the laser, and is identical to the temporal autocorrelation function of the harmonic radiation, after a time τ given by the differential propagation time of the ω and 2ω waves between the two sources. α_2 is a spatial coherence parameter of the laser. For perfect coherence, α_1 and α_1 are unity, and (4) is recovered.

We have characterized [27] the temporal and spatial coherence by measuring the SHG interferograms and extracting the α parameters. The basic principle of the experiment to determine temporal coherence is shown schematically in Fig. 8. In addition to the PSU (gas cell), an additional dispersive medium – typically fused silica

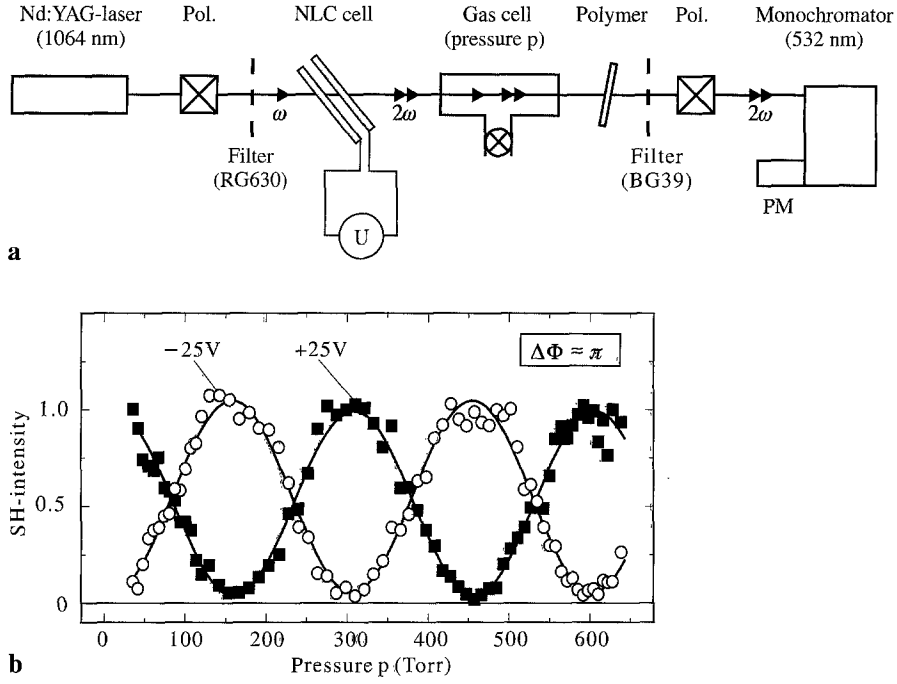

Fig. 7. Phase measurements on a nematic liquid crystal cell [22]. The NLC cell was excited by the fundamental of a Nd:YAG laser at 1064 nm with 10 mJ pulses of 8 ns duration at a repetition rate of 5 Hz as shown in **a**. The fundamental was aligned along the *p*-direction with a polarizer. A controllable phase delay was introduced by a 36 cm long gas cell filled with air at variable pressure; as the second SH source a poled polymer was chosen. The SH radiation generated in the NLC cell passed a monochromator and was detected by a photomultiplier. Using a second polarizer, it was possible to detect only the *p*-polarized component of the harmonic radiation. The two interferograms at a cell voltage $U = \pm 25$ V shown in **b** have a phase difference of approximately π indicating a sign reversal of the underlying susceptibility

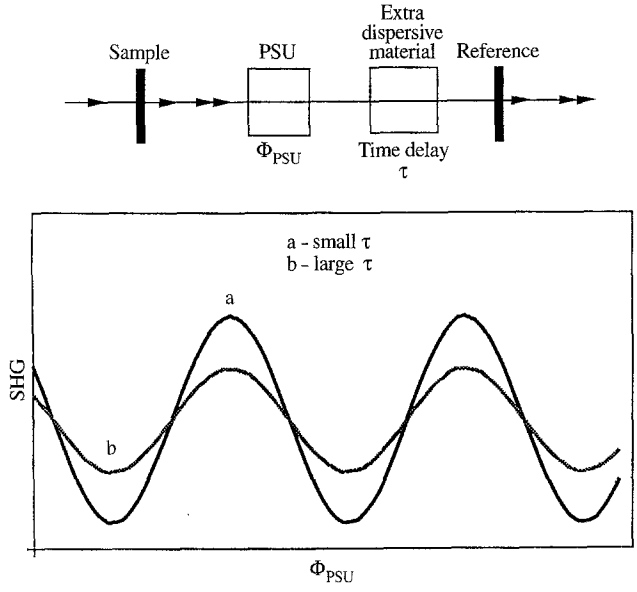

Fig. 8. Schematic for determining laser temporal coherence by SHG interference

plates – is placed between the "sample" and the "reference" SH sources. It causes an extra phase delay, equivalent to the time delay τ between the fundamental and harmonic waves. The interferograms obtained at low values of τ show highest contrast between minimum and peak total SHG, while for sufficiently large values of τ the contrast is degraded. From the dependence of the interferogram contrast on τ, the laser temporal coherence function $\alpha_1(\tau)$ can be easily deduced.

Using this technique, we have shown [27] that the temporal coherence of nanosecond pulsed *Q*-switched Nd:YAG lasers is of the order of 10 ps. Since this technique depends on a differential rather than an absolute time delay between two waves, this technique of laser coherence analysis does not have the stringent stability requirements for the optical setup necessary in most interferometric systems.

3.4 Phase measurements in total internal reflection geometry

All the SHG interference and phase measurements we have discussed so far have been performed in non-dispersive geometries, i.e. the harmonic radiation generated from the surface propagates collinearly with the residual fundamental. It is thus straightforward to perform the SHG interference because the harmonic and fundamental waves necessarily impinge on the second SH source at the same point. However, such an arrangement will clearly fail if SHG is generated in a dispersive medium or in a dispersive geometry like in Total Internal Reflection (TIR). Studies of SHG in the TIR geometry have the advantage of a much higher sensitivity due to the enhanced Fresnel factors near the critical angle [4]. Recently, SHG in the TIR geometry has been used to probe extremely weak nonlinearities at the water/oil interface [28].

For the measurement of the SHG phases in the TIR geometry, an optical compensation scheme must be employed to recombine the harmonic and residual fundamental after TIR. We have suggested and successfully demonstrated [13] two such schemes – one based on a high-index compensating prism, and the other by using a second TIR process, as shown in Fig. 9. The former scheme (Fig. 9a) was shown [13] to be easier to realize, and gave a better interferogram contrast. It has, however,

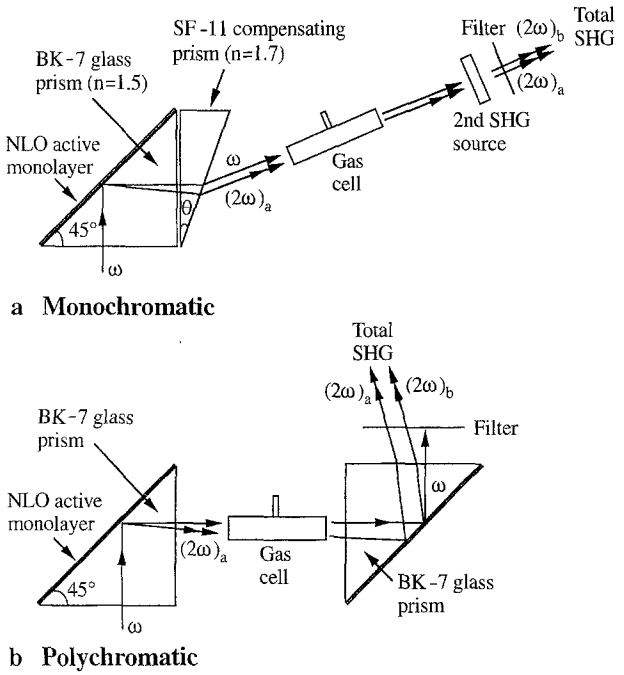

Fig. 9. Two schemes for measuring SHG interference and phases of $\chi^{(2)}$ in total internal reflection geometry. For a 1064 nm Nd:YAG fundamental and a TIR prism made of quartz, the SF-11 prism in **a** is cut with angle $\Theta = 17.5°$ to recombine the harmonic and residual fundamental after TIR. The use of a second TIR process as reference source **b** is applicable for polychromatic wavelengths but leads to a diminished interference contrast due to incomplete spatial overlap of the two harmonic beams

a disadvantage that, for each wavelength of laser operation, a different compensating prism is required. A setup employing two TIR steps (Fig. 9b) gives inferior SH interferograms due to incomplete spatial overlap of the two harmonic signals, but has the advantage that it is applicable to polychromatic wavelengths. The incomplete spatial overlap of the two harmonic beams leads to a diminished interference contrast – this effect is the spatial analogy of the incomplete temporal overlap given by the α_1 parameter of (10).

3.5 Other applications

Finally, we would like to point out that the examples mentioned are only special cases of phase-controlled nonlinear interferometry. Interference effects when fundamental and harmonic waves are created with a well-defined phase relationship from the basis of many varied studies which will now be discussed briefly. The techniques we discussed for control of the phase, and limitations due to partial laser coherence are therefore also relevant to the following studies.

Measurement of the dispersion of gases. The periodicity of the nonlinear interferogram offers probably the most accurate means of measuring the dispersion of refractive indices in gas [11].

Spectroscopy. Phase measurements have been used for spectroscopic studies on different surfaces like Langmuir-Blodgett films made of liquid crystal molecules [29] or hexadecane thiol on gold surfaces [30].

Lightfields with cube asymmetry. When waves at frequencies ω and 2ω are combined, the resultant optical electric field [31] has a time-averaged cube value $\langle E^3 \rangle \neq 0$. The magnitude and direction of this asymmetry depends on the phase difference between the two waves. Such radiation can therefore induce symmetry-breaking processes [32]. This has been verified, for example, in processes leading to the creation of bulk SHG in glass fibres [33, 34], and optical poling of molecules [35, 36].

Phase-sensitive SHG microscopy. SHG interference has been used to image domain inversion in ferroelectric crystals [37, 38]. The change of sign of $\chi^{(2)}$ upon domain inversion is imaged directly by looking at the SHG interference between the ferroelectric and a single-domain reference SHG crystal.

Mechanisms of an above-threshold ionization. Two-colour multiphoton ionization of krypton was performed using a combination of fundamental and harmonic laser photons [39]. Control of the phase between fundamental and harmonic light was shown to modulate the magnitude of Above-Threshold Ionization (ATI), enabling various theoretical models for this process to be checked [39].

Cascaded nonlinearities. As laser light propagates through a non-phase-matched SHG crystal, there is a periodic interchange of energy between fundamental and harmonic. Fundamental radiation thus emerges from the crystal with little or net loss into the harmonic mode. However, the phase of the fundamental light will be changed [40] because, in effect, it propagated partially through the crystal as harmonic radiation.

Mode locking of lasers. A nonlinear mirror, which can lead to mode locking of a Nd:YAG laser, has been demonstrated [41, 42]. The device is based on two passes through a nonlinear crystal, and adjusting the relative phase of ω and 2ω in between the two passes.

3.6 Conclusion

We have demonstrated that the measurement of the phase of the nonlinear optical response of a system is important in many applications. In direct phase measurements, the nonlinear optical signal generated by the sample is superimposed by another signal of a second (reference) sample, and a variation of the optical phase delay between these two sources results in an interference pattern from which the phase of the susceptibility can be deduced. We have compared different techniques of imparting a phase shift to control the phase difference between the input laser pulse and the nonlinear optical signal. Unless the coherence length is impractically large, the preferred method is to use a variable-pressure gas cell. Additionally, we reported on several examples of SHG phase measurements

and interferometry, including the use of phase-sensitive SHG as a probe for molecular directionality and the correct interpretation of a SH experiment when susceptibilities of different species contribute to the total SH signal. We also demonstrated that phase-sensitive SHG can be used for the measurement of coherence properties of lasers. New approaches for phase measurements in dispersive geometries are discussed.

Acknowledgement. This project has been supported by the German-Israeli Foundation For Scientific Research And Development (GIF; grant no. I-181-050.07/91). We thank A. Müller and F. Träger for a critical reading of the English version of this manuscript and also T. Dürr for technical assistance and helpful discussions.

References

1. Y.R. Shen: Nature **337**, 519 (1989)
2. R.M. Corn, D.A. Higgins: Chem. Rev. **94**, 107 (1994)
3. A. Goldmann, F. Träger (eds.): *Surface Studies by Nonlinear Laser Spectroscopies* (Springer, Berlin 1995)
4. B.U. Felderhof, A. Bratz, G. Marowsky, O. Roders, F. Sieverdes: J. Opt. Soc. Am. B **10**(10), 1 (1993)
5. R. Superfine, J.H. Huang, Y.R. Shen: Opt. Lett. **15**(22), 1276 (1990)
6. F. Geiger, R. Stolle, M. Pahlenberg, G. Marowsky: Appl. Phys. B **61**, 135 (1995)
7. G. Lüpke, G. Marowsky, R. Steinhoff: Appl. Phys. B. **49**, 283 (1989)
8. R.K. Chang, J. Ducuing, N. Bloembergen: Phys. Rev. Lett. **15**(1), 6 (1965)
9. K. Kemnitz, K. Bhattacharyya, J.M. Hicks, G.R. Pinto, K.B. Eisenthal, T.F. Heinz: Chem. Phys. Lett. **131**, 285 (1986)
10. A. Yariv: *Quantum Electronics* (Wiley, New York 1975)
11. S.P. Velsko, D. Eimerl: Appl. Opt. **25**(8), 1344 (1986)
12. J.Y. Huang, A. Lewis: Biophys. J. **55**, 835 (1989)
13. E. Schwarzberg, G. Berkovic, G. Marowsky: Appl. Phys. A **59** (6); 631 (1994)
14. R. Stolle: Aspekte von Phasenmessungen in der Nichtlinearen Optik. Ph.D. Thesis, University of Göttingen, Cuvillier Verlag Göttingen, ISBN 3-89588-252-6 (1995)
15. P. Thiansathaporn, R. Superfine: Opt. Lett. **20**(6), 545 (1995)
16. G. Marowsky, G. Lüpke: Appl. Phys. B **51**, 49 (1990)
17. M. Buck: Appl. Phys. A **55**, 395 (1992)
18. M. Buck, F. Eisert, M. Grunze, F. Träger: Appl. Phys. B **60**, 1–12 (1995)
19. D.A. Koos, G.L. Richmond: J. Chem. Phys. **93**(1), 869–871 (1990)
20. X.D. Zhu, W. Daum, X.D. Xiao, R. Chin, Y.R. Shen: Phys. Rev. B **43**(14), 11571 (1991)
21. G. Berkovic, Y.R. Shen, G. Marowsky, R. Steinhoff: J. Opt. Soc. Am. B **6**, 205 (1989)
22. R. Stolle, M. Loddoch, G. Marowsky, G. Berkovic, F.H. Kreuzer, H. Leigeber: Langmuir **11**(8), 3251 (1995)
23. O. Sato, R. Baba, K. Hashimoto, A. Fujishima: J. Chem. Phys. **95**, 9636 (1991)
24. O. Sato, R. Baba, K. Hashimoto, A. Fujishima: J. Electroanal. Chem. **95**, 291 (1991)
25. S.K. Saha, G.K. Wong: Appl. Phys. Lett. **34**(7), 423 (1979)
26. G. Berkovic, E. Schwarzberg: Appl. Phys. B **53**, 333 (1991)
27. E. Schwarzberg, G. Berkovic: Nonlinear Opt. **5**, 62 (1993)
28. J.C. Conboy, J.L. Daschbach, G.L. Richmond: J. Phys. Chem. **98**, 9688 (1994)
29. Z.-R. Tang, J.F. McGilp: J. Phys.: Condens. Matter **4**, 7965 (1992)
30. M. Buck, F. Eisert: J. Electron Spectroscopy Related Phenomena **64/65**, 159 (1993)
31. A.N. Chudinov, Yu.E. Kapitzky, A.A. Shulginov, B.Ya. Zel'dovich: Opt. Quantum Electron. **24** (1991)
32. N.B. Baranova, B.Ya. Zel'dovich, A.N. Chudinovand, A.A. Shulginov: Sov. Phys. JETP **71**, 1043 (1990)
33. B. Ehrlich-Holl, D.M. Krol, H.W.K. Tom: Opt. Lett. **17**(6), 396 (1992)
34. V. Dominic, P. Lambelet, J. Feinberg: Opt. Lett. **20**(5), 444 (1995)
35. C. Fiorini, F. Charra, J.-M. Munzi, P. Raimond: Nonlinear Opt. **9**, 339 (1995)
36. J.-M. Nunzi, F. Charra, C. Fiorinni, J. Zyss: Chem. Phys. Lett. **219**, 349 (1994)
37. F. Laurell, M.G. Roelofs, W. Bindloss, H. Hsiung, A. Suna, J.D. Bierlein: J. Appl. Phys. **71**, 4664 (1992)
38. Y. Eusu, S. Kurimura, Y. Yamamoto: Appl. Phys. Lett. **66**, 2165 (1995)
39. D.W. Schumacher, F. Weihe, H.G. Muller, P.H. Bucksbaum: Phys. Rev. Lett. **73**, 1344 (1994)
40. D.Y. Kim, W.E. Torruellas, J. Kang, C. Bosshard, G.I. Stegeman, P. Vidakovic, J. Zyss, W.E. Moerner, R. Twieg, G. Bjorklund: Opt. Lett. **19**, 868 (1994)
41. K. Stankov: Appl. Phys. B **46**, 191 (1988)
42. K. Stankov, J. Jethwa: Opt. Comm. **66**, 41 (1988)